Gyrokinetic Stability Analysis of JET Pedestal Top Plasmas with Small-ELMs

Journal of Physics: Conference Series **2397** (2022) 012007 doi:10.1088/1742-6596/2397/1/012007

Gyrokinetic Stability Analysis of JET Pedestal Top Plasmas with Small-ELMs

M. Dicorato[1,2], M. Muraglia[1], Y. Camenen[1], J. Garcia[2], X. Garbet[2], D. Frigione[3], L. Garzotti[4], P. Lomas[4], F. Rimini[4], C. Sozzi[5], and D. Van Eester[6]

[1]Aix-Marseille Université, CNRS, PIIM UMR 7345, Marseille, France
[2]CEA, IRFM, F-13108 Saint Paul Lez Durance, France
[3]National Agency for New Technologies, Energy and Sustainable Economic Development, ENEA, C.R. Frascati, Roma 00044, Italy
[4]Culham Centre for Fusion Energy of UKAEA, Culham Science Centre, Abingdon OX14 3DB, United Kingdom
[5]Istituto per la Scienza e Tecnologia dei Plasmi, 20125 Milano, Italy
[6]LPP-ERM/KMS, EUROfusion Consortium Member-Trilateral Euregio Cluster, Brussels 1000, Belgium

E-mail: mattia.DICORATO@univ-amu.fr

Abstract. In recent years, a strong effort has been dedicated to the development of tokamak plasma regimes alternative to the standard high confinement mode (H-mode) with type-I edge localized mode (ELM), i.e. ELM-free and small-ELM regimes, given the associated hardly sustainable energy and particle fluxes on plasma facing components.

In this work, we will focus on new H-mode regimes with small-ELMs, the so-called baseline small-ELMs (BSE), characterized by high thermal confinement and low core impurity accumulation, which have been recently found at JET. In order to characterize the micro-turbulence at play at the top of the pedestal, an extensive local linear gyrokinetic analysis with the GKW code has been carried out. In particular, a comparison between a reference type-I ELM (#97395) and two BSE plasmas (#96994 and #94442) has been performed.

The ion-scale ($0.1 \leq k_\theta \rho_i \leq 2$) micro-turbulence is found to have different characteristics in the two regimes. Indeed, kinetic-ballooning modes (KBM) are destabilized in the type-I ELM regime at $k_\theta \rho_i \sim 0.1$, while they are stable in BSE regimes. In addition, negative (i.e. electron-diamagnetic-direction) frequency modes, identified as electron-temperature-gradient (ETG) modes, are destabilized at $k_\theta \rho_i \sim 1.5$ in the type-I ELM regime while BSE regimes are characterized by positive (i.e. ion-diamagnetic-direction) frequency modes. Meanwhile, at electron-scale ($10 \leq k_\theta \rho_i \leq 700$) ETG modes are the dominant micro-instabilities in both regimes. Then, since BSE regimes are characterized by a higher impurity concentration at the pedestal, particular attention has been given to the role played by them. We found that impurities represent a critical player in the linear dynamics, strongly affecting the nature of micro-instabilities at ion-scale.

1. Introduction

The standard operational regime of tokamak plasmas in the last decades has been the high-confinement mode (H-mode), since its discovery in 1982 [1]. The access to this regime is enabled by the formation of an edge transport barrier (ETB), a region where particle and

heat transport are reduced. Consequently, this results in the appearance of a narrow region in the edge plasma, characterized by steep gradients (in temperature, and density), the so-called pedestal. According to the leading theory, the pedestal height and width can be determined by the combination of constraints given by low to intermediate mode number peeling-ballooning mode and larger mode number kinetic-ballooning mode (KBM) [3]. The pedestal pressure and pressure gradient growths are limited by the triggering of edge localized modes (ELMs), which are MHD instabilities responsible for quasi-periodic relaxations of the ETB.

Several types of ELMs have been observed in tokamaks and classified as a function of the heating power at which they occur and of their frequency [2]. In particular, at high input power the so-called type-I ELMs can occur. However, the energy and particle fluxes on plasma facing components due to type-I ELMs will hardly be sustainable at reactor scale.

For this reason, in recent years, a strong effort has been dedicated to the development of alternative regimes to the standard type-I ELMy H-mode while maintaining its good confinement properties, i.e. ELM-free and small-ELM regimes [4]. It is in this framework that new H-mode regimes with high frequency small-ELM, the so-called baseline small-ELMs (BSE), improved thermal confinement, and low core high-Z impurities accumulation have been developed at the Joint European Torus (JET) tokamak [5]. So far, a clear understanding of physical mechanisms responsible for the onset of BSE regimes is missing. It is then crucial to better understand the transport mechanisms responsible for the modification of the pedestal structure, which prevent the onset of type-I ELMs.

In this paper, in order to shed light on the role played by small-scale turbulent transport mechanisms in the new BSE regimes, we compare the linear stability properties of the pedestal top of three JET discharges: a reference type-I ELMy H-mode, and two BSE regimes discharges. The stability analysis is carried out by performing local linear gyro-kinetic (GK) simulations, which allow the characterization of micro-turbulence regime in term of the underlying micro-instabilities. In particular, we will find that, in agreement with the current understanding of type-I ELM regime [3], KBMs are destabilized at the top of the pedestal of the reference discharge, while they are stable in the BSE discharges, where different transport mechanisms are at play. Moreover, particular focus will be given to the role played by the impurities since BSE plasmas are characterized by a higher impurities concentration at the pedestal top with respect to the reference type-I ELM.

The next sections are organized as follows: in Section 2 the experimental conditions of the three selected discharges are summarized and compared; in Section 3 the GK framework is briefly presented and physical and numerical input parameters of the three selected discharges are detailed; in Section 4 the linear GK simulation results are presented, giving a focus on the characterization of the micro-instabilities at different scales and their dependence on driving parameters and plasma composition; in the last Section 5 a summary and discussion of the main results are given.

2. Description of the experiments: type-I ELM and two BSE discharges

The experimental setup of the three selected JET discharges are here briefly described and compared[1]. The discharge #97395 has been selected as a reference type-I ELMy H-mode in deuterium, to be compared with two different BSE regime discharges in deuterium, #96994 and #94442. In particular, discharge #96994 is characterized by a compound ELM behavior, with isolated standard big ELMs separated by longer periods of fast and smaller ELMs. While discharge #94442 is a pure small-ELMs regime obtained in different experimental conditions with respect to #96994, later discussed.

All these discharges are characterized by toroidal current $I_p = 3\,\mathrm{MA}$, toroidal magnetic field,

[1] For a complete discussion the reader is referred to Ref. [5]

JET #97395: a = 0.887 m, **JET #96994**: a = 0.87 m, **JET #94442**: a = 0.89 m

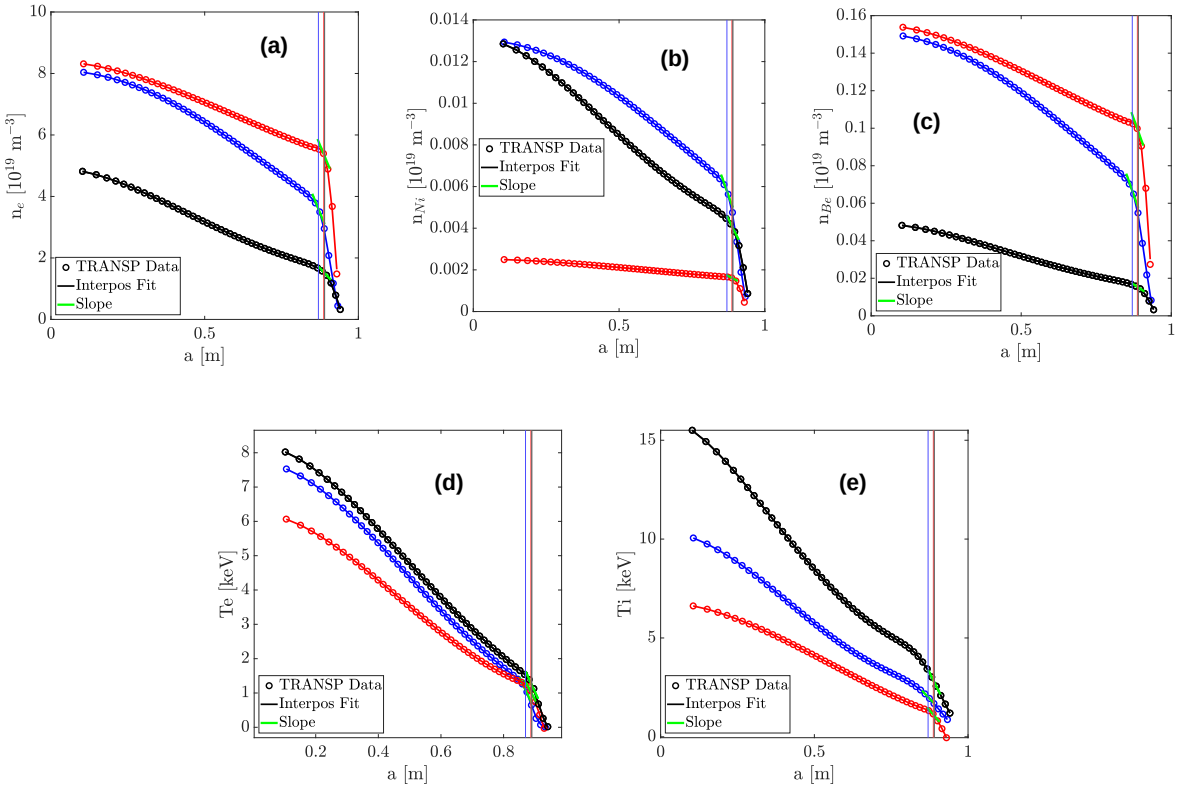

Figure 1: (a). Electron density, n_e. (b) Nickel density, n_{Ni}. (c) Beryllium density, n_{Be}. (d) Electron temperature, T_e. (e) Ion temperature, T_i. The radial locations at which the local GK simulations are performed are shown as vertical lines.

$B_t = 2.8\,\mathrm{T}$, $q_{95} = 3.2$, and low triangularity, $\delta = 0.23$. They are heated by 4 MW Ion Cyclotron Resonant Heating (ICRH) system. Neutral Bean Injection (NBI) at different powers for the three discharges has been used. A key experimental condition to access the BSE regimes is given by an optimization of deuterium neutral gas particle injection [5]. Further experimental setup are given by

- #97395. Total input power is 32 MW. The deuterium particle source is gas puff at rate $\Gamma_e(\mathrm{D}) = 2.5 \times 10^{22}\,\mathrm{s}^{-1}$.
- #96994. The total input power is 32 MW. The particle source is a mixture of D gas puff at rate $\Gamma_e(\mathrm{D}) = 0.4 \times 10^{22}\,\mathrm{s}^{-1}$, Ne injection at $\Gamma_e(\mathrm{Ne}) = 0.8 \times 10^{22}\,\mathrm{s}^{-1}$, and D pacing pellets at $f = 45\,\mathrm{Hz}$.
- #94442. The total input power is 21 MW, without gas, pellets nor Ne injection.

The plasma profiles obtained from TRANSP runs are shown in Fig. 1. Looking at the electron density profiles we notice the differences in the pedestal structures. In particular, discharge #97395 has the highest and steepest pedestal density, while the BSE plasmas have wider density pedestals. Regarding the temperature profiles, we notice that in BSE discharges higher temperatures are obtained. Moreover, at the top of the pedestal the ion to electron temperature ratio T_i/T_e, is higher for the BSE discharges than type-I ELM. Since higher temperatures in BSE regimes are achieved starting from the edge, the role of the scrape-off layer (SOL) dynamics on that is an open question and outside of this work.

Finally, we notice an important difference between the two regimes: the type-I ELM discharge is characterized by lower impurities, Be and Ni, concentrations with respect to BSE discharges. The profiles of the impurities densities are inferred in TRANSP runs assuming to be proportional to the electron density such that the ratio fulfill the constraints given by the effective charge Z_{eff} and radiated power.

3. Local gyrokinetic modelling of the pedestal top

In this work, the GKW code has been used in its local version to perform linear stability analysis of the pedestal top of the three JET discharges. Indeed, the pedestal region plays a key role in determining the confinement properties of the plasma, and it is crucial to understand the transport features in this region. We here point out that global GK simulations are typically needed to model the pedestal region. The validity of local simulations can be checked by comparing the reference Larmor radius with the gradients lengths, that in our cases $\rho_{\text{ref}}/L_{n_e} \approx 1/50$ or $\rho_{\text{ref}}/L_{T_{e,i}} \approx 1/20 - 1/50$, but as reported in Ref. [6], for these values global effects could play a role. Nevertheless, local simulations still remain a useful tool and represent a first step to investigate the pedestal stability.

In the following, a short introduction to the GKW code [7] is given. Then, the main input parameters are listed and discussed.

3.1. Brief introduction to the GKW code

The GKW code solves the coupled GK Vlasov-Maxwell system of equations in five-dimensional phase space, with three dimensions in the configuration space and two in the velocity space, for the time evolution of the perturbed distribution function δf_σ of each plasma species σ and electromagnetic fields. The equations are formulated using a field-aligned coordinate system which is well suited to resolve the turbulent structures since they are elongated along the field lines. In particular, we used the local version of the code, where the domain over which the equations are solved is given by a thin flux-tube along a magnetic field line with two coordinates perpendicular to the field line, radial and binormal respectively, and one parallel coordinate. The system of equations is solved employing an Eulerian approach, i.e. the equations are discretized on a fixed grid in the five-dimensional phase space, and integrated either by using an initial-value solver or an eigensolver.

3.2. Physical and numerical input parameters for the selected discharges

The local simulations are performed at the pedestal top of the three discharges at the radial locations shown in Fig. 1. The physical input parameters used for the gyrokinetic modelling are computed by performing cubic spline interpolations with tension, using the INTERPOS package [8], of the TRANSP plasma profiles. Plasma parameters are given in Table 1, where the normalized gradients are defined as $R/L_A = -(R_{\text{ref}}/A)(\mathrm{d}A/\mathrm{d}r)$, with A the density or temperature of a plasma species, R_{ref} the reference major radius, and $r = (R_{\max} - R_{\min})/2$ the minor radius. We can notice that most of the physical inputs for the two BSE discharges are similar while they are distinct from those of the type-I ELM discharge. The main differences are represented by the electron to ion temperatures ratio T_e/T_i, and collisionality, which are lower in BSE discharges, and the Nickel concentration, which is higher for the BSE discharges. This also affects the value of the effective charge Z_{eff}. The magnetic equilibrium is specified using a Fourier parametrization of the corresponding flux surface, with the equilibrium reconstructions provided by the TRANSP runs [9]. The simulations are performed including electromagnetic effects, i.e. parallel vector potential and parallel magnetic field fluctuations. The impact of perpendicular flow shear is not included, only the parallel flow shear drive and the Coriolis drift induced by finite toroidal rotation are. All the simulations are performed setting the ballooning

Table 1: Relevant normalized physical input parameters for local GK simulations of the three JET discharges. Here, r/R_{ref} is the inverse aspect ratio, $Z_{\text{eff}} = (\sum_\sigma n_\sigma Z_\sigma^2)/n_e$ the effective plasma charge, R/L_A the normalized gradients of density and temperature of each plasma species, q the safety factor, $\hat{s}$ the magnetic shear, $\beta_e = 2\mu_0 n_e T_e/B_{\text{ref}}^2$ the ratio of electron thermal pressure to magnetic pressure, and $\bar{\nu}_{e,i} = R_{\text{ref}}\nu_{e,i}/v_{\text{th,ref}}$ is the normalized electron-ion collision frequency. The rotation parameters are the normalized toroidal rotation velocity, $u = R_{\text{ref}}\Omega/v_{\text{th,ref}}$ where Ω is the angular velocity, and the parallel flow shear $u' = -R_{\text{ref}}^2(\partial\Omega/\partial r)/v_{\text{th,ref}}$. The reference thermal velocity is given by $v_{\text{th,ref}} = \sqrt{2T_i/m_{\text{D}}}$.

	r/R_{ref}	T_e/T_i	n_{D}/n_e	n_{Be}/n_e	n_{Ni}/n_e	Z_{eff}	R/L_{n_e}	$R/L_{n_{\text{D}}}$	$R/L_{n_{\text{Be}}}$
#97395	0.305	0.927	0.917	0.018	0.03%	1.4	12.98	12.98	12.98
#96994	0.299	0.547	0.88	0.018	0.2%	2.4	18.68	18.68	18.67
#94442	0.307	0.446	0.88	0.010	0.2%	3.1	20.63	20.63	20.55

	$R/L_{n_{\text{Ni}}}$	R/L_{T_i}	R/L_{T_e}	q	$\hat{s}$	β_e	$\bar{\nu}_{e,i}$	u	u'
#97395	12.98	47.0	48.5	3.0	2.5	0.27%	1.3165×10^{-2}	0.14	7.2
#96994	18.69	23.0	47.9	2.9	2.0	0.2%	7.55×10^{-3}	0.16	6.0
#94442	20.63	32.4	46.9	2.9	2.5	0.1%	2.18×10^{-3}	0.2	6.8

angle $\theta_0 = 0$, i.e. $k_x = 0$. Collisions are modeled using a linearized Fokker-Planck collision operator. All the plasma species are included as kinetic species.

The typical required numerical resolution for linear simulations, assessed by performing grid convergence tests, is given by $N_{\text{pol}} \times N_s \times N_{v_\parallel} \times N_\mu = 31 \times 128 \times 48 \times 32$, where $N_{\text{pol}}, N_s, N_{v_\parallel}, N_\mu$ are the number of poloidal turns, the number of grid points for each poloidal turn (the necessary value can increase up to 256 points), for the parallel velocity, and magnetic moment grids, respectively. The resolution required in the parallel direction s is much higher than typical values needed in plasma core simulations.

4. Linear simulations results

In this section the main linear GK simulation results are presented. The goal of the linear stability analysis is to characterize the micro-turbulence developed at the pedestal top of the three discharges in terms of the underlying micro-instabilities. Moreover, a comparison between the different discharges will be assessed, with the goal to better understand the differences and the critical physical mechanism at play which allows the development of BSE regimes.

The linear simulations allow to determine the growth rate γ, real frequency ω, and perturbed distribution functions of each plasma species, and the electromagnetic fields structures of the modes. A schematic summary of some typical micro-instabilities, which can appear in the pedestal region, and their features is reported in Table 2.

4.1. Full linear spectra

The simulation results obtained using the GKW initial-value solver to find the most unstable mode over a wide range of binormal wavenumbers k_θ (normalized with the main ion Larmor radius $\rho_i = m_{\text{D}} v_{\text{th,ref}}/eB_{\text{ref}}$), for the three discharges, are shown in Fig. 2.

We notice that the type-I ELM discharge is characterized by higher growth rate with respect to the BSE regimes. Then, we notice that at ion-scale a peak in the growth rate exists for the BSE regimes around $k_\theta\rho_i \sim 0.3$ and for the type-I ELM at $k_\theta\rho_i \sim 0.1$. At electron-scale all the

Table 2: Schematic of typical micro-instabilities in fusion plasmas and their features. The real frequency ω sign is positive (negative) in the ion(electron)-diamagnetic direction, according to the GKW code notation. Transport channels are particle Γ, and heat Q.

	Scale	Driven by	ω	Main transport channels	Ballooning structure
KBM	ion	R/L_p, β_e	> 0	Γ_e, Q	ballooning-parity
ITG	ion	R/L_{T_i}	> 0	Q_i, Γ_e, Q_e	ballooning-parity
TEM	ion	R/L_{T_e}, R/L_{n_e}	< 0	Q_e, Γ_e, Q_i	ballooning-parity
ETG	electron	R/L_{T_e}	< 0	Q_e, Γ_e	ballooning-parity

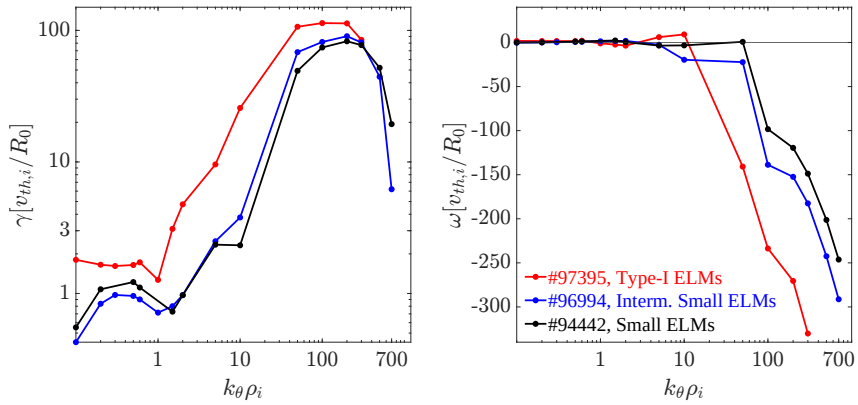

(a) Full linear spectra, ion electron scales.

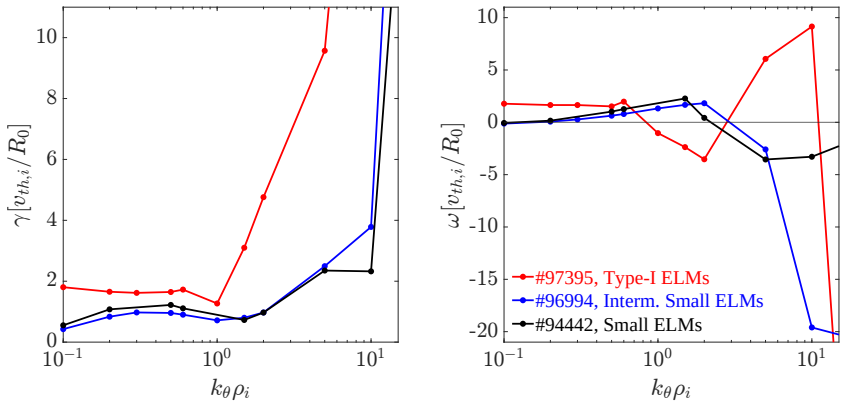

(b) Zoom at ion-scale.

Figure 2: Linear mode growth rate γ and real frequency ω spectra as a function of $k_\theta\rho_i$, at the pedestal top for the discharges #97395 in red, #96994 in blue, and #94442 in black.

discharges have a peak in the growth rate at $k_\theta\rho_i > 100$, which is typical for the plasma edge parameters [10]. In more details, the emerging physical pictures for the three discharges are given by

- #97395. At ion-scale, KBM destabilization is found at $k_\theta\rho_i \sim 0.1$. Then, an ion-temperature-gradient (ITG) mode is dominant at $k_\theta\rho_i \sim 0.5$. At electron-scale, electron-temperature-gradient (ETG) modes are the most unstable.
- #96994. At ion-scale, and up to $k_\theta\rho_i \sim 1$, a mode branch with slightly positive frequency,

increasing with $k_\theta \rho_i$, is found. Depending on the wavenumber, driving parameters associated to both ITG and trapped-electron (TE) modes are found. These features could be attributable to the "ubiquitous mode" which has been detailed investigated in Ref. [11]. Anyway, further analysis is necessary for definitive conclusion in this regard. Then, starting at $k_\theta \rho_i \sim 5$, ETG modes are dominant.

- #94442. Same picture as the previous discharge but with ETG modes dominant from $k_\theta \rho_i \sim 50$.

We notice that for both regimes the ETG branches peak at very high $k_\theta \rho_i$ resembling the recently investigated slab-ETG destabilization in JET pedestals reported in Ref. [12]. The main differences between type-I ELM and BSE regimes then appear at ion-scale. Indeed, in agreement with the current understanding of the type-I ELM regime we found that KBM is unstable in #97395 discharge, while it is stable in the BSE. Given the sensitivities of the results to the input parameters and since they have error bar associated to experimental measurements, in order to give more confidence in the obtained results, it is crucial to assess how far, in terms of the driving parameters, is the KBM destabilization in the BSE regimes. The analysis is carried out in the following.

4.2. KBM threshold analysis: scan $(\beta_e, R/L_{T_i})$

In order to study how far KBM destabilization is in the BSE discharges, #96994 and #94442, we performed a double scan in the driving KBM parameters $(\beta_e, R/L_{T_i})$. It has been done around the nominal values ($\pm 50\%$, consistent with the associated error bar) at $k_\theta \rho_i = 0.1$. The results are shown in Fig. 3. The KBM destabilization is detected as a jump in the growth rate and real frequency, to higher positive values [13].

We can see that KBM destabilization appears when increasing the nominal β_e or R/L_{T_i} by 50% for #96994 discharge, while there is no KBM destabilization for #94442. Regarding the experimental results, discharge #96994 is characterized by some isolated bigger ELMs crashes with a lower frequency with respect to the small-ELM. Meanwhile, discharge #94442 has no big ELMs crashes, suggesting some link between the lack of KBM instabilities and the appearance of small ELMs. These results give some insights on the role played by the KBM stability on transport at the pedestal top, however, the presence of KBM inside the pedestal, where the pressure gradients are higher, cannot be discarded. This will be explored in the future.

To go further, a comparison of the thermal pressure profiles of the three discharges is shown in Fig. 4. This gives a qualitative explanation of the reason why KBM are or are not destabilized. Indeed, one can notice the differences in the pedestal structures: in BSE regimes, pedestals are wider and shifted inward, with respect to type-I ELM discharge. A quantitative comparison can be done by looking at a driving parameter values for ballooning modes, e.g. the pressure gradient. In particular, a key parameter to define the stability is given by the normalized pressure gradient

$$\alpha_{\mathrm{MHD}} = -\frac{2\mu_0 R q^2}{B^2} \frac{\mathrm{d}p}{\mathrm{d}r} \, .$$

We obtain that at radial locations of our study this parameter for type-I ELM discharge is $\sim$30 % higher than #96994 discharge and $\sim$120 % higher than #94442.

4.3. The impact of impurities

Motivated by the fact that one of the main differences between the obtained plasma profiles is given by impurities concentration, a detailed analysis of the impurities effect on the linear spectra has been carried out. The results for the three discharges are shown in Fig. 5. In particular, a comparison of the growth rate and real frequency spectra of each shots including or not the impurities is detailed. In this analysis, the effects of rotation have not been taken into

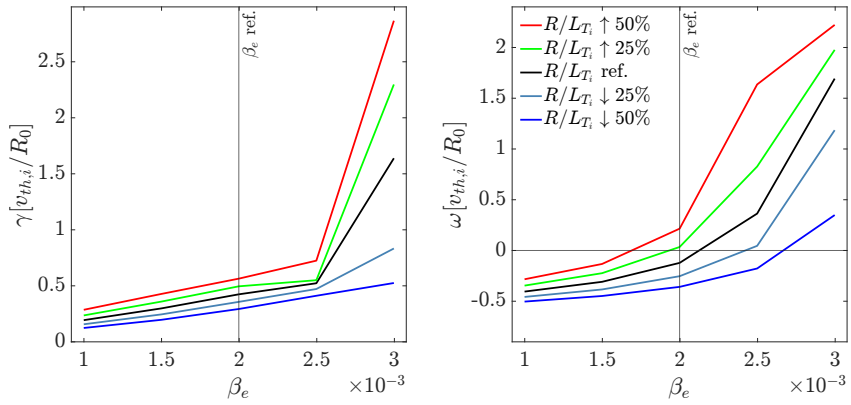

(a) #96994.

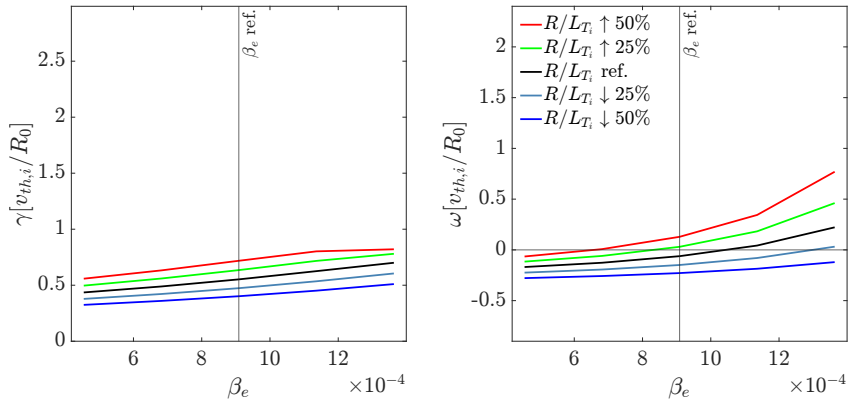

(b) #94442.

Figure 3: Linear mode growth rate γ and real frequency ω spectra as a function of β_e and R/L_{T_i} at $k_\theta \rho_i = 0.1$ of the BSE discharges. The vertical black lines indicate the experimental reference values.

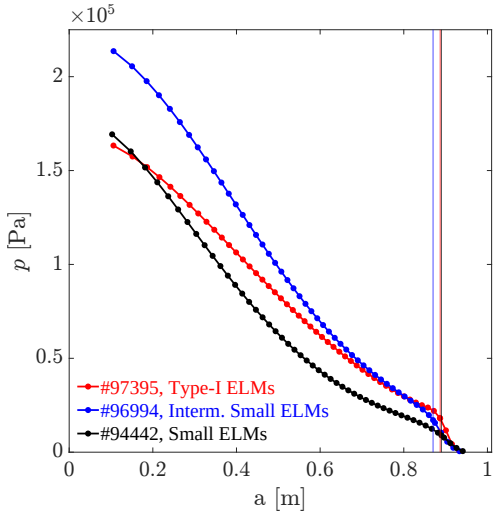

Figure 4: Pressure profiles as function of the minor radius for the three discharges. Vertical lines are at radii where analysis are performed.

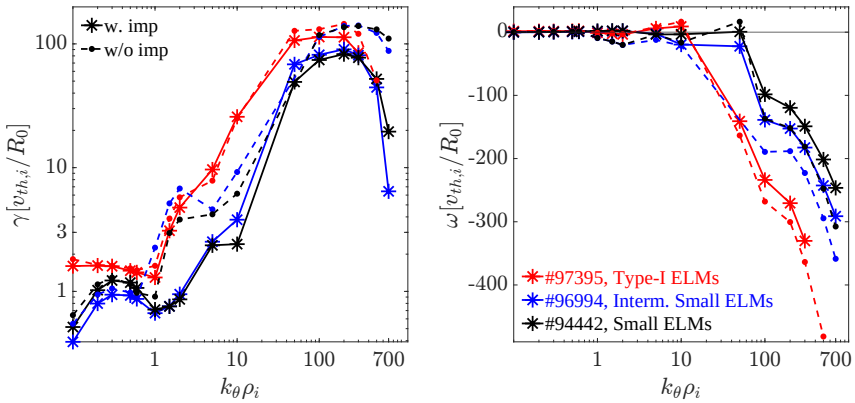

(a) Full linear spectra, ion-electron scales.

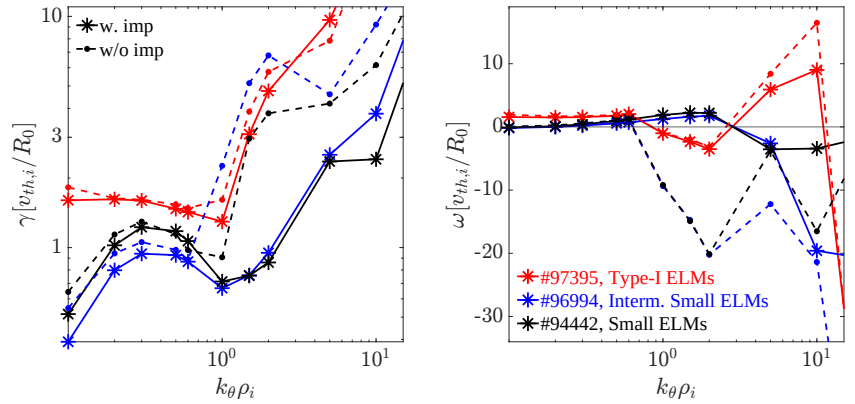

(b) Zoom at $0 < k_\theta\rho_i < 10$.

Figure 5: Linear mode growth rate γ and real frequency ω spectra as a function of $k_\theta\rho_i$ with and without impurities for the three discharges.

account, i.e. the parallel flow shear and toroidal rotation where set to zero. We notice that in type-I ELM regime, being characterized by a lower impurities concentration (see Table 1), which is regulated by ELMs flushes, the full linear spectrum is almost unaffected by the presence of impurities.

Meanwhile, in the two BSE regimes, we firstly notice that at electron-scale, $k_\theta\rho_i \sim 100$, the effect of the impurities is to reduce the growth rate without changing the nature of the mode. Instead, a strong impact due to the impurities in the range $1 < k_\theta\rho_i < 2$ of the spectra is observed. In this case the effect is twofold: a strong reduction of the growth rate, and a change in the nature of the most unstable mode, from a negative real frequency to a positive one. In particular, the effect of the impurities is to stabilize the ETG branch appearing at $1 < k_\theta\rho_i < 2$, so that the most unstable mode becomes a positive frequency impurity-driven mode. This effect can be explained by considering the role of finite Larmor radius (FLR) effects in the resonant response of the species distribution function, represented by the Bessel function $J_0(k_\perp\rho_\sigma)$, where $k_\perp$ is the perpendicular to the field line wavenumber. Since the Bessel function decays to zero as $\sim 1/\sqrt{k_\perp\rho_\sigma}$, and the Larmor radii of the plasma species satisfy the inequality $\rho_e < \rho_Z = \sqrt{A}/Z\rho_i < \rho_i$ (where for Be $\sqrt{A}/Z = 0.75$, and for Ni $\sqrt{A}/Z = 0.27$), we have that at $k_\theta\rho_i \sim 1$ without impurities the main ion response is adiabatic. On the other side, including the impurities, their resonant responses are not negligible and they give a contribution to the destabilization of the mode. As a consequence, transport features are modified by the presence of the impurities since different transport channels are activated with respect to the system

without impurities. In particular, an enhancement in particle transport is observed.

5. Summary and discussion

At JET tokamak, new H-mode plasmas with small-ELMs have been obtained [5]. These new regimes have different features with respect to standard type-I ELM, in fact they are characterized by an improved thermal confinement, and a higher impurities concentration.

In this paper we have analyzed three JET plasmas with the goal of better understanding the origin of these new BSE regimes. To this end, we have characterized, by means of linear GK simulations, the micro-instabilities at the top of the pedestal of two BSE regimes, #96994 and #94442, and we have compared it with the results obtained for a reference type-I ELM discharge, #97395. The main differences at the pedestal top of these plasmas, as reported in Table 1, are given by the level of impurities, the ratio T_e/T_i, and collisionality.

Firstly, at ion-scale we have found that KBM are destabilized in the type-I ELM discharge. Furthermore, MHD stability calculation shows that ballooning modes are destabilized too [5]. On the contrary, KBMs are stable in the BSE regimes. This suggests that the maximum achievable pressure gradient at the pedestal of BSE regimes is limited by a transport mechanism at play which prevent to reach the KBM pressure gradient threshold.

Then, motivated by the fact that one among the several differences between the pedestal top of type-I and BSE regimes is given by the impurities concentration, particular attention has been dedicated to the characterization of the role played by the impurities. We found that, for the type-I ELM discharge, they almost do not affect the linear spectrum. While for the BSE discharges they mainly affect the nature of the most unstable modes in the range $1 < k_\theta \rho_i < 2$ of the spectra, modifying the ETG branch to an impurity-driven mode, with enhanced particle transport.

A following analysis will first be a quasi-linear characterization of turbulent transport fluxes followed by a validation of the results by means of non-linear GK simulations, which in these regions of plasma parameters are very challenging and computationally demanding. Non-linear simulations will be necessary to fully characterize the micro-turbulence given by the complex interaction and competition of dominant and sub-dominant micro-instabilities, which are likely to be present given the steep gradients in the pedestal region.

Acknowledgments

The first author would like to thank Dr. M. Raghunathan for helpful discussions.

The project leading to this publication has received funding from the Excellence Initiative of Aix-Marseille University - A*Midex, a French “Investissements d’Avenir” program AMX-19-IET-013. The gyrokinetic simulations have been performed on: CINECA Marconi HPC within the project WPJET1 and Mésocentre d’Aix Marseille Université. CINECA and Center de Calcul Intensif d’Aix-Marseille are acknowledged for granting access to their high performance computing resources. This work has been carried out within the framework of the EUROfusion Consortium, funded by the European Union via the Euratom Research and Training Programme (Grant Agreements, N0 633053 and No 101052200 EUROfusion). Views and opinions expressed are however those of the author(s) only and do not necessarily reflect those of the European Union or the European Commission. Neither the European Union nor the European Commission can be held responsible for them.

References

[1] Wagner F, Becker G, Behringer K, Campbell D, Eberhagen A, Engelhardt W, Fussmann G, Gehre O, Gernhardt J, Gierke G v, Haas G, Huang M, Karger F, Keilhacker M, Klüber O, Kornherr M, Lackner K, Lisitano G, Lister G G, Mayer H M, Meisel D, Müller E R, Murmann H, Niedermeyer H, Poschenrieder W, Rapp H, Röhr H, Schneider F, Siller G, Speth E, Stäbler A, Steuer K H, Venus G, Vollmer O and Yü Z 1982 *Phys. Rev. Lett.* **49**(19) 1408–1412 URL `https://link.aps.org/doi/10.1103/PhysRevLett.49.1408`

[2] Zohm H 1996 *Plasma Physics and Controlled Fusion* **38** 105–128 URL https://doi.org/10.1088/0741-3335/38/2/001
[3] Snyder P, Groebner R, Hughes J, Osborne T, Beurskens M, Leonard A, Wilson H and Xu X 2011 *Nuclear Fusion* **51** 103016 URL https://doi.org/10.1088/0029-5515/51/10/103016
[4] Viezzer E 2018 *Nuclear Fusion* **58** 115002 URL https://doi.org/10.1088/1741-4326/aac222
[5] Garcia J, de la Luna E, Sertoli M, Casson F, Mazzi S, Ž Štancar, Szepesi G, Frigione D, Garzotti L, Rimini F, van Eester D, Lomas P, Sozzi C, Aiba N, Dicorato M, Mariani A, Coelho R, Frasinetti L, Huijsmans G and Liu F 2022 *Physics of Plasmas* **29** 032505 URL https://doi.org/10.1063/5.0072236
[6] Candy J, Waltz R E and Dorland W 2004 *Physics of Plasmas* **11** L25–L28 (*Preprint* https://doi.org/10.1063/1.1695358) URL https://doi.org/10.1063/1.1695358
[7] Peeters A, Camenen Y, Casson F, Hornsby W, Snodin A, Strintzi D and Szepesi G 2009 *Computer Physics Communications* **180** 2650–2672 ISSN 0010-4655 URL https://www.sciencedirect.com/science/article/pii/S0010465509002112
[8] Sauter O and SPC-EPFL , private communication *(a publication is under development)*
[9] Candy J 2009 *Plasma Physics and Controlled Fusion* **51** 105009 URL https://doi.org/10.1088/0741-3335/51/10/105009
[10] Told D, Jenko F, Xanthopoulos P, Horton L D and Wolfrum E 2008 *Physics of Plasmas* **15** 102306 URL https://doi.org/10.1063/1.3000132
[11] Coppi B and Pegoraro F 1977 *Nuclear Fusion* **17** 969–993 URL https://doi.org/10.1088/0029-5515/17/5/009
[12] Parisi J F, Parra F I, Roach C M, Giroud C, Dorland W, Hatch D R, Barnes M, Hillesheim J C, Aiba N, Ball J, Ivanov P G and contributors J 2020 *Nuclear Fusion* **60** 126045 URL https://doi.org/10.1088/1741-4326/abb891
[13] Snyder P B and Hammett G W 2001 *Physics of Plasmas* **8** 744–749 URL https://doi.org/10.1063/1.1342029